Computer Aided Geometric Design 43 (2016) 131–142

Contents lists available at ScienceDirect

Computer Aided Geometric Design

www.elsevier.com/locate/cagd

Efficient Voronoi diagram construction for planar freeform spiral curves

Jaewook Lee [a], Yong-Jun Kim [b], Myung-Soo Kim [c,*], Gershon Elber [d]

[a] Dept. of Electrical and Computer Engineering, Seoul National University, Seoul 08826, South Korea
[b] Digital Factory Division, Siemens PLM, Ann Arbor, MI 48105, USA
[c] Dept. of Computer Science and Engineering, Seoul National University, Seoul 08826, South Korea
[d] Computer Science Department, Technion, Haifa 32000, Israel

ARTICLE INFO

Article history:
Available online 15 February 2016

Keywords:
Voronoi diagram
Medial axis
Planar freeform curve
Spiral curve
Moebius transformation
Maximal disk

ABSTRACT

We present a real-time algorithm for computing the Voronoi diagram of planar freeform piecewise-spiral curves. The efficiency and robustness of our algorithm is based on a simple topological structure of Voronoi cells for spirals, which also enables us a direct construction of Voronoi structure without relying on intermediate polygonal or biarc approximations to the given planar curves. Using a Möbius transformation, we provide an efficient search for maximal disks. The correct topology of Voronoi diagram is computed by sampling maximal disks systematically, which entails subdividing spirals until each belongs to a pair/triple of spirals under a certain matching condition. The matching pairs and triples serve as the basic building blocks for bisectors and bifurcations, and their connectivity implies the Voronoi structure. We demonstrate a real-time performance of our algorithm using experimental results including the medial axis computation for planar regions under deformation with non-trivial self-intersections and the Voronoi diagram construction for disconnected planar freeform curves.

1. Introduction

Voronoi diagram is a partition of space into cells, each containing points closer to a specific site than to any other sites (Aurenhammer, 1991; Okabe et al., 2000). Common boundaries of adjacent Voronoi cells can be used for the construction of Medial Axis Transform (MAT) or Skeleton, a powerful shape descriptor originally introduced by Blum (1967, 1973). Nevertheless, the skeleton may not always be constructed by removing some redundancies from the common boundaries. (There may be certain skeletal parts missing from the Voronoi edges when some non-convex sites have self-bisectors in the interior of their Voronoi cells.) To avoid this problem, we consider sites which are spirals. (Spiral curve is a curvature monotone planar curve with no inflection point in the curve interior Barton and Elber, 2011; Meek and Walton 1995, 1999.) Spirals provide many useful geometric properties for the development of efficient and robust algorithms for planar curves (Aichholzer et al. 2009, 2010; Lee et al. 2015a, 2015b; Oh et al., 2012).

Regarding the construction of Voronoi diagram and medial axis for planar freeform curves, the segmentation into spirals makes the computation of topological structures very stable (Aichholzer et al. 2007, 2009, 2010; Aigner, 2007). Motivated by the theoretical guarantee on the convergence of the medial axis for spiral biarc spline approximation to the exact medial

* Corresponding author.
E-mail address: mskim@snu.ac.kr (M.-S. Kim).

http://dx.doi.org/10.1016/j.cagd.2016.02.008
0167-8396/

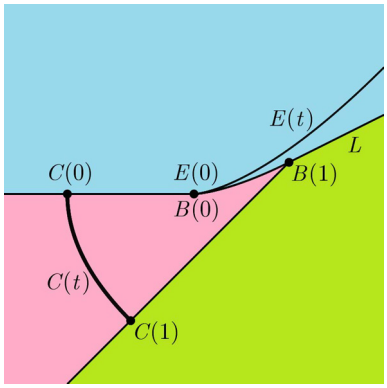

Fig. 1. A spiral curve $C(t) = \left(\frac{1}{2}t^2, -t\right)$, $0 \le t \le 1$, and its Voronoi diagram: the regions of different color correspond to the Voronoi cells of $C(0)$, $C(1)$, and the curve interior. (For interpretation of the references to color in this figure, the reader is referred to the web version of this article.)

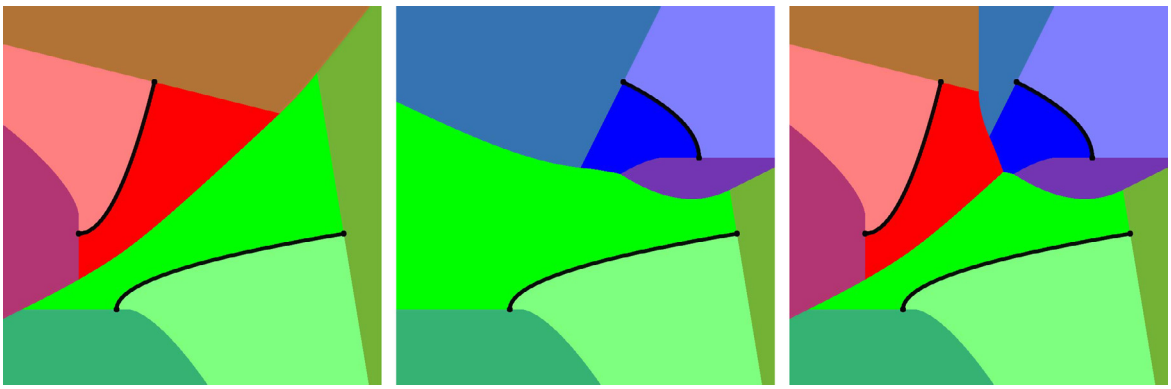

Fig. 2. Voronoi diagram for three spiral curves and their endpoints. (For interpretation of the references to color in this figure, the reader is referred to the web version of this article.)

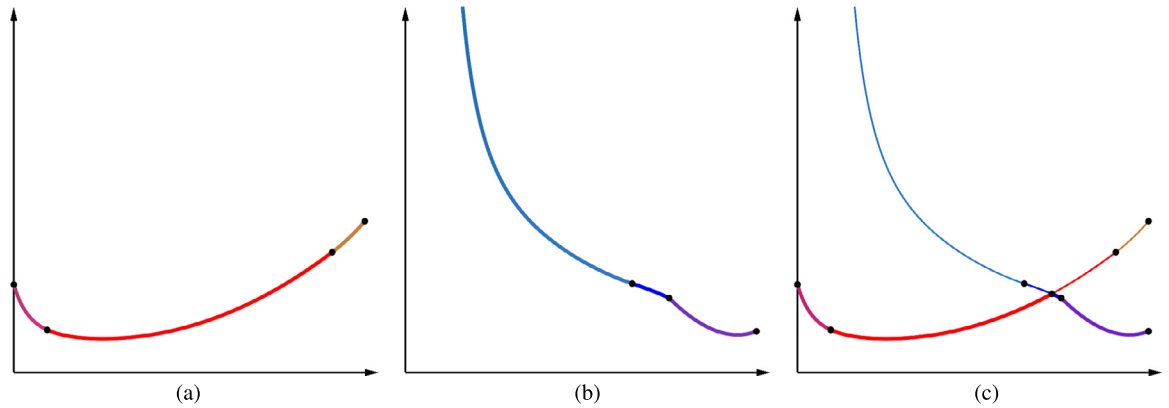

Fig. 3. Lower envelope of distance maps.

axis of the original curve (Aichholzer et al., 2007; Aigner, 2007), we develop an algorithm that accelerates the construction of Voronoi cells for planar spiral curves by directly computing the correct topology of Voronoi diagram using a small number of properly sampled maximal touching disks to the original freeform curves. The theoretical guarantee on the correct topology (in a finite number of sampling steps) also leads to the efficiency and robustness of our algorithm in practice. The bifurcation locations can be computed precisely using a numerical method (Hu and Wallner, 2005). The sequence of bisectors connecting bifurcations and terminals can be constructed very efficiently (within a given Hausdorff error bound) using the conic bisectors between spiral biarc approximations to the given planar curves (Aichholzer et al. 2007, 2009, 2010; Aigner, 2007).

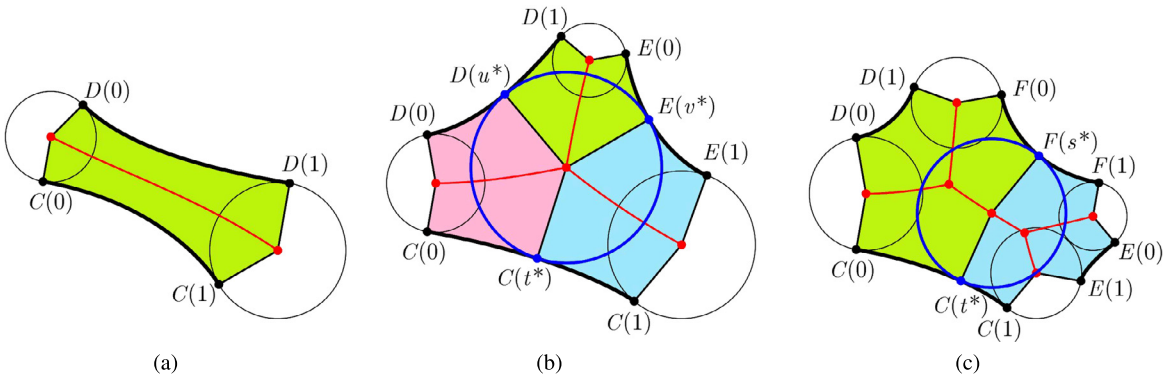

Fig. 4. Colored region R for a matching pair or triple: (a) two matching curves, (b) three matching curves subdivided to three pairs of matching curves, and (c) four matching curves subdivided to two triples of matching curves. (For interpretation of the references to color in this figure, the reader is referred to the web version of this article.)

Before proceeding with the algorithm, we first illustrate a few simple examples. Given a spiral $C(t) = \left(\frac{1}{2}t^2, -t\right)$, $0 \le t \le 1$, Fig. 1 shows three Voronoi cells that correspond to the disjoint sites: $s_0 = \{C(0)\}$, $s_1 = \{C(t) \mid 0 < t < 1\}$, and $s_2 = \{C(1)\}$. The curve $B(t) = \left(1 + \frac{3}{4}t^2, \frac{1}{4}t^3\right)$, $0 < t < 1$, is a bisector between a point s_0 and the curve s_1, and the borderline L (between the Voronoi cells for s_0 and s_2) is on the bisector between $C(0)$ and $C(1)$. The evolute curve of $C(t)$, i.e., $E(t) = \left(1 + \frac{3}{2}t^2, t^3\right)$, is totally contained in the Voronoi cell of $C(0)$; thus the spiral $C(t)$, $0 < t < 1$, has no self-bisector in its own Voronoi cell. This example is generic in the sense that all inflection-free spiral curves (also monotone along the x and y directions) have the same Voronoi cell structure as the one shown in Fig. 1.

Overlaying two simple Voronoi diagrams for spirals, we can construct the Voronoi diagram for two spiral curves. As shown in Figs. 2(a)–(b), each Voronoi cell for a spiral is bounded by relatively simple bisector curves and there appears no bifurcation point (with three or more branches) where three different curve–curve bisectors can meet. As shown in Fig. 2 with different colors, it is convenient to treat the convex and concave sides of a spiral curve $C(t)$ as different sites, i.e., $C^+(t)$ and $C^-(t)$, with their respective normals facing to two opposite directions. Curve endpoints are considered as circular arcs spanning angle π but with radius 0. When two spirals share a common endpoint at a sharp corner, we assign a range of normal angles to the convex side of the point, but no angle to the concave side. Similarly, when two spirals intersect transversally at a point, we split them into four spirals and assign no angle to the intersection point as the four sides are all concave.

Now to discuss the case of three spirals (which may have a bifurcation), we use the lower envelope concept of Hanniel et al. (2007), which provides a direct translation of the definition of Voronoi cell to a graphical form. Fig. 3(a) shows the lower envelope of the distance maps from the spiral (except the endpoints) in the lower right to the bisectors with the spiral (including the two endpoints) in the upper left (see Fig. 2(a)). Note that the lower envelope represents the distance maps to three different bisectors, two point-curve bisectors and one curve–curve bisector. Similarly, Fig. 3(b) shows the lower envelope of the distance maps from the lower-right spiral to another spiral in the upper right (see Fig. 2(b)). Finally, Fig. 3(c) shows the lower envelope of the two lower envelopes, which represents the distance maps from the lower-right spiral to the bisectors with the other two spirals (see Fig. 2(c)). In this example, there is a crossing between the first two lower envelopes, which corresponds to a bifurcation for the three spirals. One may wonder why there exists a unique bifurcation for this configuration of three spirals. We answer this question below.

Figs. 4(a)–(b) show the two base cases of our algorithm. An initial setup of our algorithm (Section 5) will clear other spirals from the colored region. Then, the first case of two matching spirals has no bifurcation (Fig. 4(a)). Using the lower envelope of the distance maps from $C(t)$ to the bisectors with $D(u)$ and $E(v)$, the existence of bifurcation can be shown for the second case (Fig. 4(b)). The uniqueness of bifurcation is a direct consequence of splitting a matching triple to three matching pairs (Fig. 4(b)), where each pair produces no further bifurcation. The existence of a unique bifurcation for each matching triple plays a pivotal role in the acceleration of our spiral-based algorithm and also in computing the correct topology of Voronoi diagram. By sampling maximal disks in a systematic way (see Fig. 4(c) and more details in Section 5), the bifurcation problem (for computing the correct topology) can be reduced to a number of subproblems, where each belongs to one of two base cases: (i) a matching pair of spirals with no bifurcation (Fig. 4(a)) or (ii) a matching triple of spirals with a unique bifurcation (Fig. 4(b)).

For an efficient computation of maximal disk O_t, we introduce a Möbius transformation that converts all tangent circles to parallel lines and reduces the problem to a numerical search in the parameter domain of a scalar function (see more details in Section 4). In the final stage of the Voronoi diagram construction, we approximate the bisectors with low degree curves (e.g., conics). (The exact bisectors are, in general, algebraic curves of extremely high degree, Elber and Kim, 1998.) For estimating the Hausdorff distance error in the bisector approximation, Aichholzer et al. (2009) used an upper bound: $4\epsilon/[1 - \cos(\xi/2)]$, where ξ is the angle between the two lines from the center of O_t to the two touching points. As this

bound can be very large for a small value of ξ, in Section 5.3, we develop a different method that bounds the error more efficiently in this special case.

The rest of this paper is organized as follows. In Section 2, we briefly review related previous work on computing the Voronoi diagram and the medial axis for planar freeform curves. We then explain the basic ideas in Section 3, by illustrating the construction steps for a simple example. Section 4 presents a transformation technique that converts the search for maximal disk to a function optimization problem. In Section 5, we discuss how to construct the Voronoi cells of spirals with a correct topology of bifurcations and also bound the Hausdorff distance error in the bisector curve approximation. Some experimental results are presented in Section 6, and finally, Section 7 concludes the paper.

2. Related work

Early developments (mostly in the area of computational geometry) for computing the Voronoi diagram and medial axis transformation of discrete objects (such as points, line segments, polygons, polyhedra, and even circles and circular arcs) are very well documented in an extensive literature survey of Aurenhammer (1991). This section thus mainly focuses on the Voronoi diagram and medial axis constructions and other related geometric computations on planar freeform curved objects.

Lavender et al. (1992) made the first attempt to construct the Voronoi diagram for general curved sites, given as set-theoretical solid models. Using a divide-and-conquer construction scheme for set models, the algorithm generates the Voronoi diagram in a quadtree/octree representation. In the case of handling planar sites in 2D, the same representation can be computed considerably more efficiently in real-time using a graphics hardware-based method of Hoff et al. (1999). Nevertheless, the precision of geometric computation is limited to an image resolution as is often the case in the majority of image processing applications.

For CAD/CAM applications, Chou (1995) proposed a solution to the medial axis construction for planar simply-connected curved regions, where a fast numerical method was used for tracing the bisector curves on the medial axis. Farouki and Ramamurthy (1998) presented a bisector tracing technique using the envelope of point-curve bisector curves. By marching along the boundary curves (instead of tracing along the bisector curves on the medial axis), Ramanathan and Gurumoorthy (2003) extended the medial axis construction to the general multi-connected planar curved regions possibly with interior holes. In the current work, we also take an approach that moves along each spiral curve but the conceptual paradigm is based on the lower envelope scheme for the Voronoi cell construction of Hanniel and Elber (2009) while the spiral curves greatly simply the envelope structure of distance maps.

Seong et al. (2008) focused on the construction of bifurcation points by solving a set of polynomial equations. Using osculating circles of spirals, we present an efficient method for computing bifurcation points, which can be made numerically stable even for degenerate cases based on the curvature monotonicity of spiral. Though not needed for the current work, the saddle point computation of Cao et al. (2011) can also be significantly accelerated and numerically stabilized using osculating circles of spirals.

Spiral segmentation accelerates many other distance-related geometric computations as well. For example, using the properties of spiral, Oh et al. (2012) greatly simplified the point projection problem, i.e., the problem of projecting points to the nearest footpoints on the planar rational curves. Using a dynamic bounding volume hierarchy of bounding circular arcs (BCAs) efficiently generated for deformable spiral curves, Lee et al. (2015a) accelerated the offset curve trimming for planar freeform curves. There are also other types of tight bounding volumes such as spiral fat arcs (Barton and Elber, 2011) and bilens (Kurnosenko, 2013) which have great potential in accelerating other types of geometric computations. Spiral segmentation also provides a handy tool for proving the cubic convergence of biarc approximation to freeform planar curves (Meek and Walton 1995, 1999).

Choi et al. (1997) introduced an important construction paradigm, the so-called domain decomposition, which greatly simplifies the medial axis computation for planar regions. They used maximal disks to split the medial axis into simple components. Based on the domain decomposition paradigm, Aichholzer et al. (2009, 2010) introduced a spiral biarc-based approach to develop an efficient and robust algorithm for computing the medial axis of planar freeform shapes. The G^1-continuity of biarcs eliminates many artifacts arising from the polygonal approximation of planar curves. Moreover, the spiral biarc approximation is essential in the preservation of the topological structure of medial axis (Aichholzer et al., 2007; Aigner, 2007).

Motivated by the preservation of topology under spiral biarc approximation (Aichholzer et al., 2007; Aigner, 2007), we take a direct approach to computing the correct topology of Voronoi diagram. We show that some important properties of the spiral biarc-based approach Aichholzer et al. (2009, 2010) can be preserved to our case using relatively simple topological arguments. The main advantage of our spiral-based algorithm is that we have only two base cases (i.e., matching pairs or triples) to consider and they can be determined more efficiently.

3. Example of medial axis construction

We explain the basic construction steps for our algorithm using an illustrative example. Fig. 5(a) shows a planar simply-connected region bounded by a closed cubic B-spline curve. The boundary curve is first segmented into inflection-free

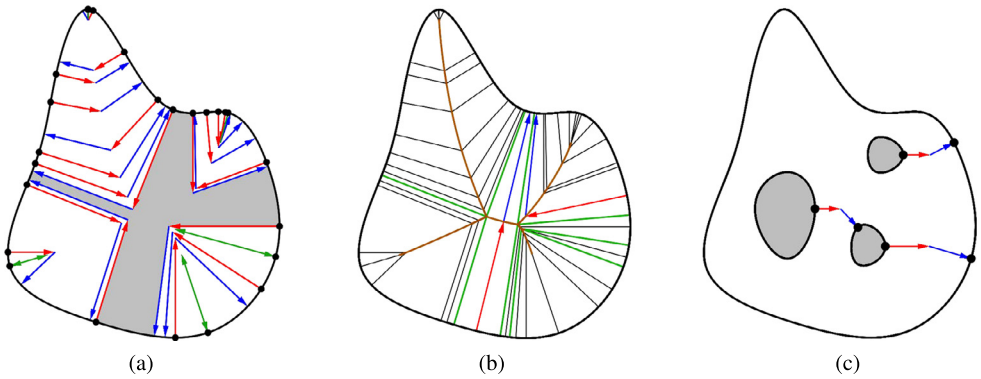

Fig. 5. Example of medial axis construction. (For interpretation of the references to color in this figure, the reader is referred to the web version of this article.)

curvature monotone spirals which are also monotone along the x and y-directions. At each endpoint of spiral, the maximal disk is computed. The mapping from each endpoint (black dot) to the disk center (red arrow) and then to the other touching point (blue arrow) is shown in Fig. 5(a). We further segment the spirals at the touching points. The curvature maximum (convex) endpoints are shown with bidirectional arrows (green) to the centers of osculating maximal disks, which correspond to the terminal points of the medial axis.

When two spirals $C(t)$ and $D(u)$ share the same maximal disks at their endpoints, they form a matching pair and generate a bisector curve segment on the medial axis. The bisector between two matching spirals has no self-intersection, i.e., no bifurcation may occur in this part of the medial axis.

Now we consider three spirals $C(t)$, $D(u)$, $E(v)$, each pair of which share only one maximal disk at their respective endpoints. The three spirals form a matching triple and they generate a bifurcation point with three branches of bisectors, each of which is generated by a pair of spirals. The bifurcation point is the center of a common tangent disk to the three spirals. The existence of bifurcation for a matching triple can be proven using the lower envelope of two distance maps (see related discussions in Introduction). By subdividing the three spirals at their touching points (with the common tangent disk), we have three matching pairs of spirals, each of which generates a bifurcation-free bisector segment. This proves the uniqueness of bifurcation for a matching triple.

In Fig. 5(a), there is one matching triple (with the rightmost endpoint and the rightmost green arrow), which is special in that two spirals share not only the same maximal disk but also their common endpoint. This triple generates a terminal point as well as a bifurcation. Fig. 5(a) also shows a region (shaded) with a matching quadruple of spirals. When we subdivide the spiral on the right, the four-spiral region is reduced only in size but not in the number of spirals. Subdividing the spiral at the bottom, we can finally split the region into two subregions, each with a matching triple of spirals. Fig. 5(b) shows the result of medial axis construction after the above two subdivisions of spirals. The topology of medial axis is the same as the connection structure of the matching pairs and triples. Multiply-connected regions can be handled in a similar way by converting them to simply-connected ones as shown in Fig. 5(c).

Replacing spirals by spiral biarcs, we can show that the matching conditions and the uniqueness of bifurcation also hold in the same way. This is a direct proof for the preservation of topology under spiral biarc approximation (Aichholzer et al., 2007; Aigner, 2007).

4. Efficient search for maximal disk

Each interior point $\mathbf{p}$ on an oriented spiral curve $C(t)$ has a unique normal line $L_N(t)$ along the normal direction $N(t)$ of the curve. The maximal disk touching at $\mathbf{p}$ will have its center located on the normal line $L_N(t)$. Once we can efficiently compute the radius of maximal disk for each $\mathbf{p}$, the Voronoi diagram construction is essentially done for the spiral curve $C(t)$. For the sake of simplicity of presentation, by translation and rotation if necessary, we assume $\mathbf{p}$ is located at the origin $(0,0)$ and the curve $C(t)$ is tangent to the y-axis at the origin and with $(1,0)$ as its unit normal. The circles tangent at the origin $(0,0)$ is given in the following form:

$$(x-r)^2+y^2=r^2, \quad \text{or} \quad \frac{x^2+y^2}{2x}=r>0.$$

If the maximal circle has another contact point at a different spiral curve $D_i(u)=(x_i(u),y_i(u))$, $0\le u\le 1$, the corresponding radius $r>0$ will be the minimum among all such values:

$$r=\min_u\left[\frac{x_i^2(u)+y_i^2(u)}{2x_i(u)}\right]>0.$$

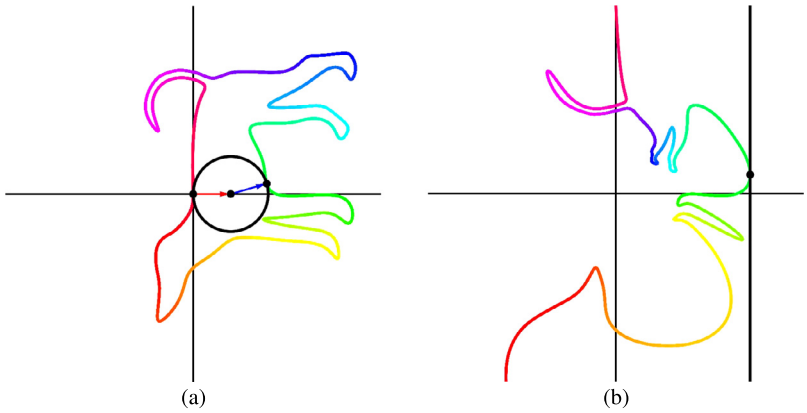

Fig. 6. Inversion of the maximal inscribed tangent circle to the rightmost tangent line along the y-direction.

The search for the minimum radius can be done equivalently by the search for the maximum of its reciprocal:

$$1/r = \max_u \left[\frac{2x_i(u)}{x_i^2(u) + y_i^2(u)} \right] > 0.$$

There are some computational advantages of taking this reciprocal approach. First of all, there needs no special consideration of the case $x_i(u) \le 0$ and this function converges to the radius of curvature of $C(t)$ when $D_i(u)$ is taken as the curve $C(t)$ itself and $u \to t$. (In the current work for spirals only, we filter out these cases from further consideration; but these properties are useful for other distance-related applications.) More importantly, the inversion $1/\mathbf{z}$ (of the representation $\mathbf{z}$ of a point (x, y) as a complex number $\mathbf{z} = x + yi$) transforms all circles tangent at $(0, 0)$ to the y-axis to lines parallel to the y-axis and all other circles to circles, and thus bounding circular arcs of $D_i(u)$ to similar ones (except those containing the origin $(0, 0)$, which can easily be detected and replaced by others). Fig. 6 shows the result of inverting a planar closed curve, where the maximal circle is converted to the rightmost tangent line along the y-direction. As in this example, it is usually relatively easy to find the range of parameters $[u_1, u_2]$ where the exact touching parameter u of $D_i(u)$ is contained (e.g., via a simple overlap test for a hierarchy of bounding circular arcs of $D_i(u)$ against a tangent disk slightly larger than the maximal disk). The parameter u itself can be found more efficiently using numerical iterations near the exact solution.

5. Construction of the Voronoi diagram

We first start with computing maximal disks at the endpoints of all spirals. For the sake of simplicity in designing algorithm and proving its correctness, we assume that all spiral curves are segmented into non-self-intersecting, inflection-free, and x and y-monotone pieces, and each is further segmented into smaller pieces at the touching points of maximal disks constructed in the initial step. (See more details in Section 6.)

5.1. Voronoi cell for a spiral curve

Given a spiral $C(t)$ $(0 \le t \le 1)$, we consider a matching spiral $D(u)$ $(0 \le u \le 1)$, sharing a maximal disk O_0 touching at $C(0)$ and $D(0)$, and similarly a matching spiral $E(v)$ $(0 \le v \le 1)$, sharing a maximal disk O_1 touching at $C(1)$ and $E(1)$. (We assume that the proper side of each spiral is under consideration with suitable reparameterization. Degenerate circular arcs of radius 0 are also treated as spirals in a similar manner.) There are three different cases to consider.

1. $D(u)$ and $E(v)$ are the same spiral. (This means that $C(t)$ and $D(u)$ form a matching pair.) Then there should be no other spiral in the region R bounded by $C(t)$, $D(u)$, and the two disks O_0 and O_1 (see Fig. 4(a)). Suppose there were some other spirals inside R; then, the maximal disks at some spiral endpoints (e.g., the y-extreme endpoints among these other spirals) would touch $C(t)$ or $D(u)$ in the curve interior. This is a contradiction to the segmentation of $C(t)$ and $D(u)$ so that no further touching point could appear in the curve interior. By inserting the bisector of $C(t)$ and $D(u)$ in the middle of R, the Voronoi cell for $C(t)$ can be constructed, and similarly for $D(u)$.
2. $D(u)$ and $E(v)$ share a maximal disk $\hat{O}$ touching at $D(1)$ and $E(0)$. (This means that $C(t)$, $D(u)$, and $E(v)$ form a matching triple.) Then we detect a bifurcation point where the maximal disk O_t of $C(t)$ $(0 \le t \le 1)$, changes the matching curve from $D(u)$ to $E(v)$ at some $t = t^*$. (See Fig. 4(b).) We discuss more details in Section 5.2.
3. Otherwise, there is a unique sequence of spirals C_i's, $i = 1, \cdots, N$ (starting from $C_1 = D$ and ending at $C_N = E$), where each pair of consecutive spirals share a maximal disk at their proper endpoints. We show that the problem can be reduced to the base cases of matching pairs and triples, or to subproblems of smaller size by recursive subdivision, which provides a proof by construction for the termination of algorithm. There are three different cases to consider.

(a) There exists a common tangent disk for $C(t)$, $D(u)$, $E(v)$ which is also a maximal disk for $C(t)$ at some curve interior. Then we break each of $C(t)$, $D(u)$, $E(v)$ into two pieces at their respective touching parameters $t = t^*$, $u = u^*$, $v = v^*$. (See the discussion in Section 5.2.) By inserting bisectors, we construct the Voronoi cells for $C(t)$ $(0 \le t \le t^*)$, and $D(u)$ $(0 \le u \le u^*)$, and also the Voronoi cells for $C(t)$ $(t^* \le t \le 1)$, and $E(v)$ $(v^* \le v \le 1)$. The problem is reduced to a subproblem with a shorter sequence of spirals.

(b) The common tangent disk exists but contains some other spiral in its interior. As shown in Fig. 4(c), we compute the maximal disk O^* of $C(t)$ at the touching parameter $t = t^*$, and find the matching spiral $F(s)$ $(0 \le s \le 1)$. (Since there are only a finite number of spirals, $F(s) = C_k(s)$, for some $2 \le k \le N-1$; otherwise, we could construct another sequence of matching C_i's from D to E, which is impossible.) After breaking each of $C(t)$ and $F(s)$ into two pieces at the touching parameters $t = t^*$ and $s = s^*$, we repeat the construction recursively with two reduced subproblems, each with a shorter sequence of C_i's. At the end of the recursion, we will end up with each subproblem with only three spirals to deal with.

(c) There is no common tangent disk for $C(t)$, $D(u)$, $E(v)$ (e.g., when $D(u)$ and $E(v)$ are very short and almost flat). Using a bisection search, we can find a matching spiral $C_k(s)$, for some $2 \le k \le N-1$, and repeat the construction.

5.2. Detecting bifurcations

Given a matching triple of spirals $C(t)$, $D(u)$, $E(v)$, each pair of which sharing a maximal disk at their respective endpoints, we first compute a common tangent disk O^* to the three spirals at some parameters: $0 < t = t^*$, $u = u^*$, $v = v^* < 1$, and the disk interior contains no part of these spirals. (An argument similar to the case of a matching pair can show that there can be no other spiral in the colored region R of Fig. 4(b).) We break each of $C(t)$, $D(u)$, and $E(v)$ into two pieces at $t = t^*$, $u = u^*$, and $v = v^*$. By inserting bisectors, we construct the first-half Voronoi cell for $C(t)$ $(0 \le t \le t^*)$, using the bisector with $D(u)$ $(0 \le u \le u^*)$, and the second-half Voronoi cell for $C(t)$ $(t^* \le t \le 1)$, using the bisector with $E(v)$ $(v^* \le v \le 1)$. The Voronoi cells for $D(u)$ and $E(v)$ can also be constructed in a similar way.

A common tangent circle to three spirals can be computed using a generalized version of the Apollonius problem (Elber and Kim, 2001). Instead of solving a system of trivariate polynomial equations, in the current work, we apply a numerical improvement procedure to three sequences of osculating circles to the spirals $C(t)$, $D(u)$, $E(v)$, and efficiently compute the common tangent circle with a correct orientation to the three osculating circles. The touching points on the osculating circles are then projected back to the three spirals (Hu and Wallner, 2005) and the iteration can be repeated. The approach of using osculating circles has been observed to be numerically stable; nevertheless, the convergence to the exact solution can be slowed down in various situations where the osculating circles do not provide a good approximation to the real geometry. In the case of slow convergence, we switch to a bisection method which guarantees at least a linear convergence to the exact solution.

The bisection approach is also a good method of choice for resolving numerical instabilities that may arise in this problem. In the case of multiple matching spirals $C(t)$, $D(u)$, $E(v)$, $F(s)$, $\cdots$, by subdividing at the mid-parameter of each spiral in this order and iterating if necessary, we can end up with the base cases of matching pairs and triples. Degenerate bifurcation, with four or more branches at the same point, can be detected from a common tangent circle that touches some spiral(s) other than the three constructor spirals.

5.3. Bounding Hausdorff distance error in bisector construction

Aichholzer et al. (2009) approximated the exact bisector curve using the bisectors (conics) for spiral biarc approximation to the boundary curve. They used an upper bound: $4\epsilon/[1-\cos(\xi/2)]$, for estimating the Hausdorff distance error in the bisector construction, where ϵ is the error in the spiral biarc approximation and $\xi \in [0, \pi]$ is the angle between the two lines from the disk center to the two touching points on the matching spirals. This closed-form formula provides an efficient algorithm for bounding the bisector approximation error. Nevertheless, when the angle ξ approaches to zero, the upper bound can be unnecessarily large. Thus, for the case of small values of ξ, we develop a different method for bounding the error tightly.

The exact bisector of two spirals is totally contained in the common intersection of the Voronoi cells for the two spirals. Fig. 1 shows that the Voronoi cell for the concave side of $C(t)$ is bounded by two line segments and a bisector curve $B(t)$. Replacing $B(t)$ by the chord line segment connecting $B(0)$ and $B(1)$, we can generate a slightly enlarged region, bounded by $C(t)$ and three line segments. (Any superset of Voronoi cell may serve for the purpose of enclosing the exact bisector.) Fig. 7 shows two examples where the exact bisector is contained in a quadrangle, which is the intersection of two such supersets (each enclosing the respective Voronoi cell). In Fig. 7(a), the left corner of the yellow quadrangle is the bisector terminal point and the right corner is the intersection between the two normal lines at the other (curvature-minimum) endpoints of two spirals. On the other hand, in Fig. 7(b), the left corner is the intersection between two normal lines at the inner (curvature-maximum) endpoints of two spirals. The thickness of quadrangle provides a simple upper bound for the Hausdorff distance error in the bisector curve approximation. The examples of Fig. 7 illustrate typical cases where a small value of ξ may occur. Two almost flat concave spirals sharing a common endpoint at their curvature maximum may generate an almost linear bisector curve, for which our geometric error bound provides an effective way of estimating the approximation error.

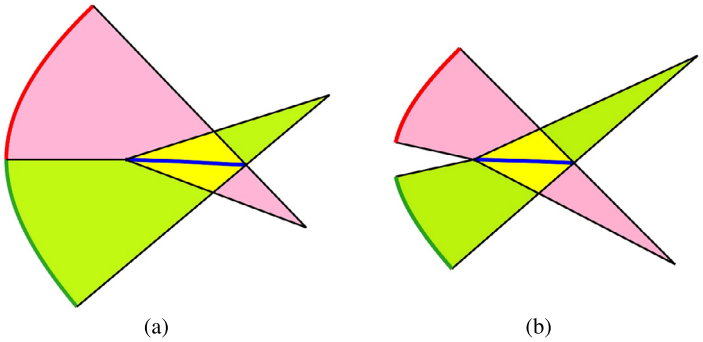

Fig. 7. Exact bisector is contained in a quadrangle. (For interpretation of the references to color in this figure, the reader is referred to the web version of this article.)

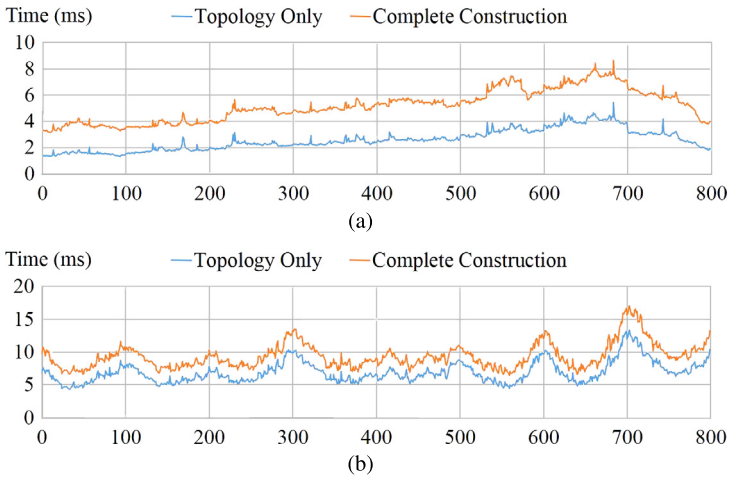

Fig. 8. Computing time for the correct topology and the total construction complete with bisector approximation: (a) the medial axis and (b) the Voronoi diagram, where the horizontal axis displays the frame numbers of the 800 test examples in an animation sequence, some snapshots of which are shown in Figs. 9 and 10.

In the current work, employing the bisector construction method of Aichholzer et al. (2009), we approximate the exact bisector (typically high-degree algebraic curves) using the exact bisectors (conics) of spiral biarc approximation. Even in the case of small values of ξ, the spiral biarcs produce their bisectors (conics) within the geometric error bound estimated by our method discussed above. In the case of small values of ξ, we can alternatively use biarcs (conics) interpolating the boundary conditions of exact bisectors, as it is quite easy to test the containment of biarcs in bounding quadrangles. This is the approach we have taken in our experiments to be reported in the following section.

6. Experimental results

We have implemented our Voronoi diagram construction algorithm in C++ on an Intel Core i7-4790 3.6GHz PC with an 8GB main memory. To demonstrate the effectiveness of our approach, we have tested our algorithm to the same 800 examples of planar freeform curves that had been used in the experiments of Lee et al. (2015a) for offset curve trimming, where the spiral segmentation was also applied to the freeform curves in each example. (Details of the test results are reported in Figs. 8–10.) Some of these planar curves have non-trivial self-intersections and sharp corners. (The computation of all self-intersection points can be done efficiently using a hierarchy of bounding circular arcs in a similar way as in the offset self-intersection computation, Lee et al., 2015a. Moreover, sharp corners are handled as degenerate arcs in the same way as they were used for generating circular offset arcs.) This means that the medial axis (in the conventional sense) may not be well-defined for the self-intersecting curves. Nevertheless, there are still a finite number of closed regions, each bounded by piecewise continuous planar freeform curves. We compute the medial axis for each of these bounded planar regions using the Voronoi cell structure for the spirals on the boundary freeform curves.

Fig. 8(a) reports the computing time for determining the correct topology of medial axes for the bounded planar regions (in each of the 800 examples), and a complete medial axis construction within a given Hausdorff distance error bound of 10^{-5}, where all the freeform curves are defined in the normalized window of $[-1, 1] \times [-1, 1]$. Both the topology and the

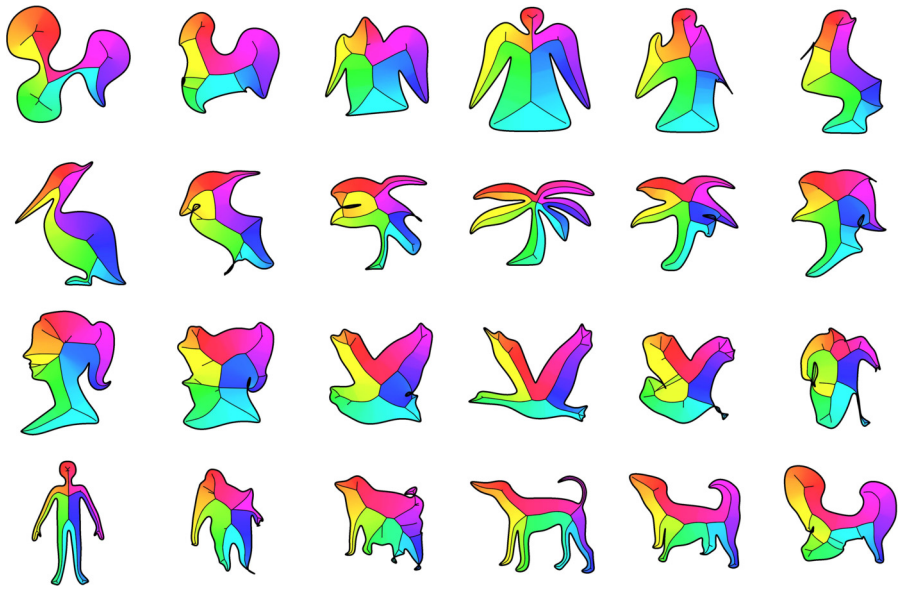

Fig. 9. Snapshots of medial axis construction for planar regions bounded by deformable planar periodic B-spline curves.

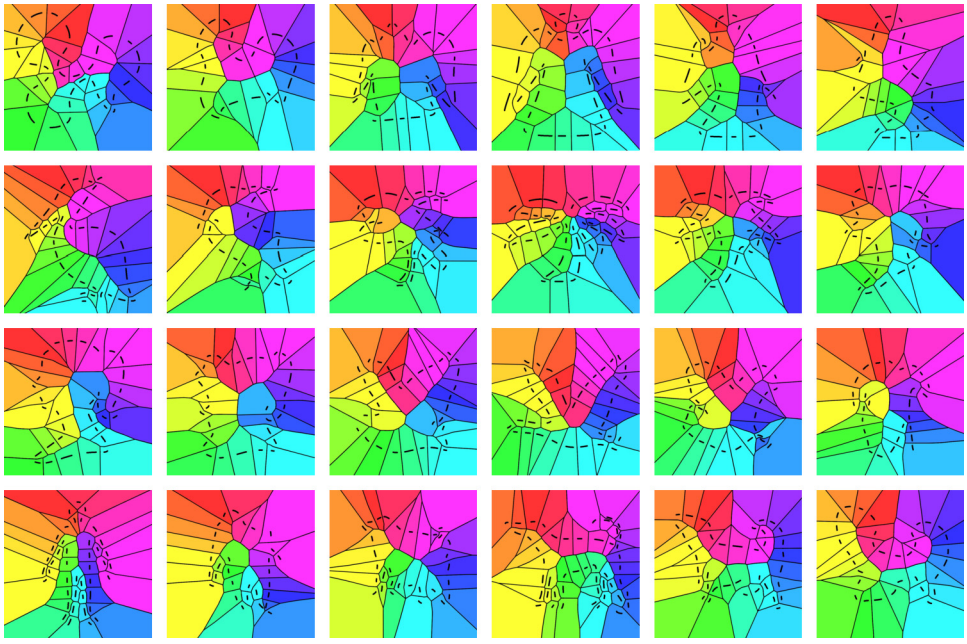

Fig. 10. Snapshots of Voronoi diagram construction for deformable planar disconnected B-spline curves.

bisector curve approximations (using conics) for each of these complex examples can be computed in real-time. Fig. 9 shows 24 snapshots taken from the 800 construction results of medial axes for planar bounded regions.

By taking only alternating curve segments from a connected sequence of piecewise continuous curves in each example, we can generate a large number of disconnected freeform curves, each of which can be considered as a degenerate closed planar region of empty area. Fig. 8(b) reports a real-time performance for computing the correct topology of Voronoi diagram for these disconnected planar freeform curves, and also a construction of Voronoi diagram, complete with the bisector curve's approximations (using conics), within a given Hausdorff distance error bound of 10^{-5}. Fig. 10 shows 24 snapshots taken from the 800 construction results of the Voronoi diagram.

Fig. 11 shows the results from testing the medial axis algorithm to four highly complex planar shapes. Because of the large input size, it is difficult to support a real-time performance for these test models. The table at the bottom of each example shows (i) the number of control points for a periodic cubic B-spline curve, (ii) the number of spirals, (iii) the computing time for determining the correct topology, and (iv) the total computing time for the medial axis construction

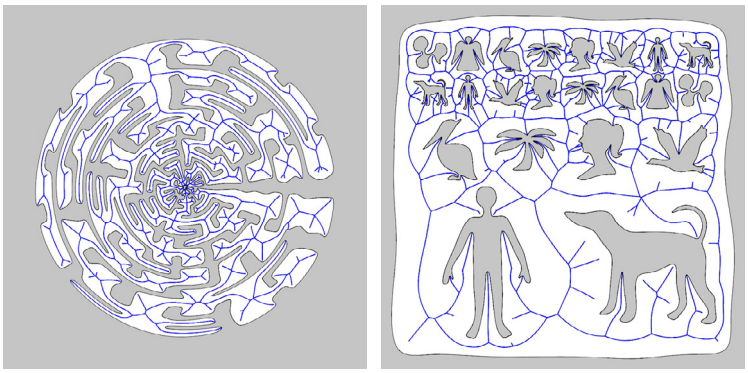

#CPts	#Spirals	Topology	Complete
1306	2994	54 ms	90 ms

(a)

#CPts	#Spirals	Topology	Complete
2132	3906	90 ms	124 ms

(b)

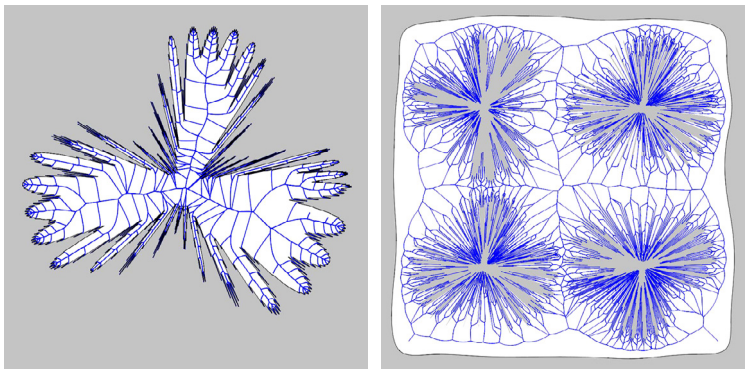

#CPts	#Spirals	Topology	Complete
2000	4747	177 ms	240 ms

(c)

#CPts	#Spirals	Topology	Complete
8032	17144	730 ms	902 ms

(d)

Fig. 11. Medial axis construction for highly complex examples.

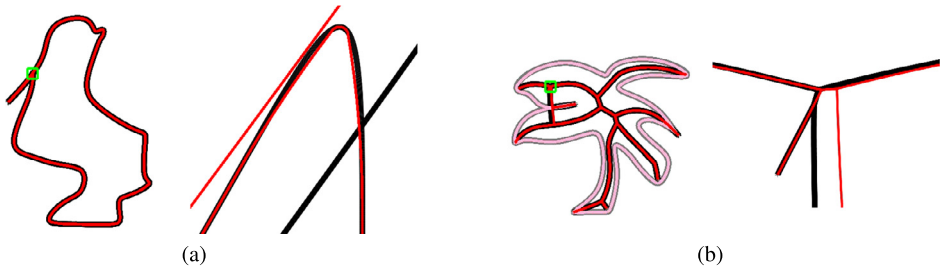

(a) (b)

Fig. 12. Change of topology in (a) the boundary curve approximation and (b) the medial axis. (For interpretation of the references to color in this figure, the reader is referred to the web version of this article.)

complete with the bisector approximation. Though the example of Fig. 11(c) has a smaller number of B-spline control points than the example of Fig. 11(b), the medial axis construction takes more computing time. Because of many sharp corners, the shape complexity increases with a larger number of spirals. Even in this fractal-like non-trivial test example, our spiral-based algorithm has produced a high-precision medial axis construction with the correct topology in a numerically stable way. In this specific fractal model, the input size can be changed by controlling the recursion level of the fractal generation. Using the fractal models of different size thus generated, we have observed the expected asymptotic performance of $O(n \log n)$ in computing time for the medial axis construction, where n is the number of spirals and the factor of $O(\log n)$ is due to the divide-and-conquer style approach of our algorithm and the binary searches in the hierarchy of various bounding volumes.

A direct construction algorithm for the Voronoi structure has advantages over the conventional methods relying on polygonal or biarc approximations. Even in the case of highly reliable previous algorithms (Aichholzer et al. 2007, 2009, 2010; Aigner, 2007), where the convergence to the correct topology is guaranteed, it is unknown a priori which precision could determine the correct topology. Fig. 12 shows two examples (frames 169 and 275) from the 800 test data discussed

above. A small region in the green box of Fig. 12(a) is expanded in the right subfigure, where the biarc approximation (in red) has a different topology from the self-intersecting boundary curve (in black). A careful examination is needed for the preservation of input topology in the biarc approximation. A more difficult case is shown in Fig. 12(b), where the topology of bifurcation in the medial axis is changed in the construction with a biarc approximation. A careful analysis on the separation of bifurcations is needed to determine the correct topology. A simple solution to this problem might be to use a spiral biarc approximation of sufficiently high precision. Nevertheless, it is not easy to decide the required high precision. In contrast to this limitation, our algorithm can determine the correct topology as the result of spiral segmentations until each spiral belongs either to a matching pair or to a matching triple.

7. Conclusion

We have presented an efficient and robust algorithm for computing the Voronoi diagram of planar freeform curves and the medial axis of planar regions bounded by freeform curves. Monotone spiral segmentation of the input freeform curves and the maximal disks computed at the spiral endpoints greatly simplified the Voronoi cell construction algorithm for each spiral. The efficiency and numerical stability of the proposed approach will be useful in many 2D shape processing applications that are based on the medial axis structure such as the recent work of Zhu et al. (2014). In the future work, we plan to extend the Voronoi cell construction of Hanniel and Elber (2009) for planes, spheres, and cylinders to the general Voronoi cell construction for arbitrary freeform surfaces.

Acknowledgements

The authors would like to thank the anonymous reviewers and the program co-chairs for their invaluable comments, which were very useful in improving the overall structure of this paper, in particular, by the addition of a new Section 3 on the basic construction steps for the medial axis of an illustrative example. This work was supported in part by the Israel Science Foundation (grant No. 278/13), and also in part by the Korean MCST and KOCCA in the CT R&D Program 2014 (No. R2014060001), and in part by National Research Foundation of Korea Research Grants (No. 2013R1A1A2010085).

References

Aichholzer, O., Aurenhammer, F., Hackl, T., Jüttler, B., Oberneder, M., Sir, Z., 2007. Computational and structural advantages of circular boundary representation. In: Dehne, F., Sack, J.R., Zeh, N. (Eds.), Algorithms and Data Structures. In: Lect. Notes Comput. Sci. Springer, pp. 374–385.

Aichholzer, O., Aigner, W., Aurenhammer, F., Hackl, T., Oberneder, M., Jüttler, B., 2009. Medial axis computation for planar free-form shapes. Comput. Aided Des. 41 (5), 339–349.

Aichholzer, O., Aigner, W., Aurenhammer, F., Hackl, T., Jüttler, B., Pilgerstorfer, E., Rabl, M., 2010. Divide-and-conquer for Voronoi diagrams revisited. Comput. Geom. 43 (8), 688–699.

Aigner, W., 2007. The medial axis of planar shapes. Master Thesis. Institute for Theoretical Computer Science, University of Technology, Graz, Austria.

Aurenhammer, F., 1991. Voronoi diagrams – a survey of a fundamental geometric data structure. ACM Comput. Surv. 23 (3), 345–405.

Barton, M., Elber, G., 2011. Spiral fat arcs – Bounding regions with cubic convergence. Graph. Models 73 (2), 50–57.

Blum, H., 1967. A transformation for extracting new descriptors of shape. In: Wathen-Dunn, W. (Ed.), Models for the Perception of Speech and Visual Form. MIT Press, pp. 362–380.

Blum, H., 1973. Biological shape and visual science (Part I). J. Theor. Biol. 38 (2), 205–287.

Cao, L., Ba, W., Liu, J., 2011. Computation of the medial axis of planar domains based on saddle point programming. Comput. Aided Des. 43 (8), 979–988.

Choi, H.I., Choi, S.W., Moon, H.P., Wee, N.-S., 1997. New algorithm for medial axis transform of plane domains. Graph. Models Image Process. 59 (6), 463–483.

Chou, J., 1995. Voronoi diagrams for planar shapes. IEEE Comput. Graph. Appl. 15 (2), 52–59.

Elber, G., Kim, M.-S., 1998. Bisector curves of planar rational curves. Comput. Aided Des. 30 (14), 1089–1096.

Elber, G. Kim, M.-S., 2001. Geometric constraint solver using multivariate rational spline functions. In: Proc. of ACM Symposium on Solid Modeling and Applications. Ann Arbor, MI, June 4–8, pp. 1–10.

Farouki, R., Ramamurthy, R., 1998. Specified-precision computation of curve/curve bisectors. Int. J. Comput. Geom. Appl. 8 (5–6), 599–617.

Hanniel, I., Elber, G., 2009. Computing the Voronoi cells of planes, spheres and cylinders in R^3. Comput. Aided Geom. Des. 26 (6), 695–710.

Hanniel, I., Ramanathan, M., Elber, G., Kim, M.-S., 2007. Precise Voronoi cell extraction of free-form planar piecewise C^1-continuous closed rational curves. Int. J. Comput. Geom. Appl. 17 (5), 453–486.

Hoff, K., Culver, T., Keyser, J., Lin, M.C., Manocha, D., 1999. Fast computation of generalized Voronoi diagrams using graphic hardware. In: Proc. of SIGGRAPH 99. In: Comput. Graph. Proc. Annu. Conf. Ser., pp. 277–286.

Hu, S.-M., Wallner, J., 2005. A second order algorithm for orthogonal projection onto curves and surfaces. Comput. Aided Geom. Des. 22 (3), 251–260.

Kurnosenko, A., 2013. Biarcs and bilens. Comput. Aided Geom. Des. 30 (3), 310–330.

Lavender, D., Bowyer, A., Davenport, J., Wallis, A., Woodwark, J., 1992. Voronoi diagrams of set-theoretic solid models. IEEE Comput. Graph. Appl. 12 (5), 69–77.

Lee, J., Kim, Y.-J., Kim, M.-S., Elber, G., 2015a. Efficient offset trimming for deformable planar curves using a dynamic hierarchy of bounding circular arcs. Comput. Aided Des. 58 (1), 248–255.

Lee, J., Kim, Y.-J., Kim, M.-S., Elber, G., 2015b. Comparison of three bounding regions with cubic convergence to planar freeform curves. Vis. Comput. 31 (6–8), 809–818.

Meek, D., Walton, D., 1995. Approximating smooth planar curves by arc splines. J. Comput. Appl. Math. 59 (2), 221–231.

Meek, D., Walton, D., 1999. Spiral arc spline approximation to a planar spiral. J. Comput. Appl. Math. 107, 21–30.

Oh, Y.-T., Kim, Y.-J., Lee, J., Kim, M.-S., Elber, G., 2012. Efficient point projection to freeform curves and surfaces. Comput. Aided Geom. Des. 29 (5), 242–254.

Okabe, A., Boots, B., Sugihara, K., Chiu, S.-N., 2000. Spatial Tessellations: Concepts and Applications of Voronoi Diagrams, 2nd ed. John Wiley & Sons, Chichester.

Ramanathan, M., Gurumoorthy, B., 2003. Constructing medial axis transform of planar domains with curved boundaries. Comput. Aided Des. 35 (7), 619–632.
Seong, J.-K., Cohen, E., Elber, G., 2008. Voronoi diagram computations for planar NURBS curves. In: Proc. of the 2008 ACM Symp. on Solid and Physical Modeling. June 2–4. Stony Brook, New York, USA, pp. 67–77.
Zhu, Y., Sun, F., Choi, Y.-K., Jütler, B., Wang, W., 2014. Computing a compact spline representation of the medial axis transform of a 2D shape. Graph. Models 76 (5), 252–262.